Received: 13 November 2021 | Revised: 30 December 2021 | Accepted: 2 January 2022

DOI: 10.1002/apj.2744

RESEARCH ARTICLE

Asia-Pacific Journal of Chemical Engineering | Curtin University | WILEY

Suppression of thermoacoustic instability and NOx emissions of unsteady swirl premixed flame with upstream microjets

Liubin Hu | **Hao Zhou**

Institute for Thermal Power Engineering, State Key Laboratory of Clean Energy Utilization, Zhejiang University, Hangzhou, China

Correspondence
Hao Zhou, Institute for Thermal Power Engineering, State Key Laboratory of Clean Energy Utilization, Zhejiang University, Hangzhou, 310027, China.
Email: zhouhao@zju.edu.cn

Funding information
National Science Fund for Distinguished Young Scholars, Grant/Award Number: 51825605

Abstract

Passive control methods are widely used in unsteady combustion systems due to their robustness and convenience. This paper used the upstream microjets method for the first time to control thermoacoustic instability and pollutant NOx emissions in unsteady swirl premixed flame. Three variables of CO_2 microjets flow rate, upstream microjets distance, and microjets number are investigated. Results demonstrate the upstream microjets distance plays a significant role in restraining the thermoacoustic instability and NOx emissions. The smaller the upstream microjets distance, the more completely the thermoacoustic instability is suppressed while the NOx emissions are the opposite, which means a compromise choice needs to be made between them. The damping ratio of pressure amplitude in the chamber can reach the maximum of 81.3%, and the damping ratio of CH* intensity can reach the maximum of 80.2%. Besides, the frequency of pressure and CH* will transit to a lower mode. NOx emissions can realize a maximum reduction of 12.2 ppm. Meanwhile, the flame mode switches from an enlarged Mode-A flame to a shrunk Mode-B flame, and the flame length shows a maximum reduction of 14 mm at the largest upstream distance. However, the specific control mechanism under upstream microjets still needs further study to clarify. This research proved the feasibility of suppressing combustion instability and NOx emissions with upstream microjets in unsteady swirl premixed flame, promoting its practical application in gas turbine systems.

KEYWORDS

flame mode, NO_x emissions, thermoacoustic instability, unsteady swirl premixed flame, upstream microjets

1 | INTRODUCTION

As a complex multidisciplinary problem, combustion instability was first proposed by scholar Rayleigh.[1] When combustion instability occurs, it is often accompanied by periodic large pressure oscillations.[2,3] The power engines in gas turbines, industrial furnaces, and rockets will face the threat of damage or even failure.

To prevent the occurrence of combustion instability, researchers often implement control strategies from the two necessary factors of combustion instability, namely, acoustic oscillations and heat release oscillations. For

acoustic oscillations, the acoustic energy is dissipated in the form of heat by adding perforated liners[4] or plates,[5] quarter-and half-wave tubes,[6] Helmholtz resonators,[7] and baffles in the burner,[8] thereby breaking the phase coupling between sound waves and heat release.[9] The rich vortex structure, such as shear-layer vortices, counter-rotating vortices, and horseshoe vortices in the crossflow jet,[10] can be used to control the thermoacoustic instability driven by vortex shedding. Among them, Choi et al.[11] experimented on suppressing combustion oscillation and noise by injecting secondary fuel into the local flame structure. They found the pressure fluctuations and NOx emissions could be controlled for the case of pure methane injection, while the effectiveness is limited by injecting fuel with air. Ghoniem et al.[12] compared the controlling effect of stability and emission with air injection and H_2 addition in premixed combustion. A sufficient momentum air jet in crossflow will reduce the pressure amplitude by up to 12 dB and turn the NOx emission to the single ppm levels. The addition of H_2 will also improve the flame stability while slightly increasing the NOx emissions. Murat Altay et al.[13] examined the controlling effect of combustion instability with two different air injection configurations. The first configuration is applied with a row of microjets in the cross-stream direction, located upstream of the step. The second configuration consists of an array of microjets in the streamwise direction, located on the face of the step. Combustion instability could be suppressed, and the flame would anchor slightly upstream of the step with the first configuration. Combustion instability could be mitigated at an optimum secondary air flow rate when injecting air in the streamwise direction. LaBry et al.[14] clarified the correlation between thermoacoustic instability and vortex shedding in the swirl combustor. Their results indicated counter-swirling microjets could eliminate instability and stabilize the inner recirculation zone between modes of instability. Altay et al.[15] investigated the suppression effect of combustion instability with cross-stream air injection from a slot or microjets near the step of a backward-facing step combustor. The experiments are examined when the fuel bar is located 35 cm or 95 cm upstream of the step. They demonstrated the fuel bar location had a significant impact on the combustion dynamics. Both the slot and the microjets could mitigate the instability when the fuel bar was located 35 cm upstream of the step. However, the microjets became less valuable when the fuel bar was located further upstream of the step. In the above research, air and H_2 are widely used as traditional jet media.

Recently, CO_2 dilution from the exhaust gas recirculation (EGR) technique[16–18] serves as a low-cost and easy-to-implement combustion control and emission reduction method. Studies have shown that the unique physical and chemical properties of CO_2[19–22] have a significant impact on combustion kinetics and pollutant emissions. Gascoin et al.[19] used a modified CHEMKIN code and a radiation code to simulate the thermal effect of CO_2 on NOx formation in a methane diffusion flame. They found the addition of CO_2 could reduce the flame temperature, which limited the formation of NOx. The replacement of N_2 by CO_2 could effectively suppress NOx formation mainly due to thermal effects, followed by its chemical and radiation effects. Wang et al.[20] simulated the chemical effect of CO_2 on CH_4 and H_2 spherical flames with an open-source CFD package laminarSMOKE. The results showed the chemical effect of CO_2 could decrease the unstretched flame propagation speed. Hasti et al.[23] evaluated the chemical kinetics effect of CO_2 dilution on the CH_4/air jet turbulent flame structure with the help of a large eddy simulation (LES). The flame length will increase with the CO_2 levels resulting from a decrease of turbulent flame speed. Soloklou et al.[24] numerically analyzed the CO_2 dilution on non-premixed methane/air laminar flame with finite volume method (FVM). They found that the flame length decreases linearly with the CO_2 rising, beneficial for a shorter combustion chamber. Besides, the NOx emissions will fall by the CO_2 increase.

In terms of experiments, researches on CO_2 dilution can be found in papers.[25–32] Lee et al.[25] compared the dilution effects of N_2, CO_2, and steam on the combustion performance of H_2-CO flame. Their results indicated 40% dilution of N_2, CO_2, and steam could decrease NOx by 79%, 88%, and 95%, respectively. Moreover, the combustion efficiency is good in most of the tested cases. Sahu et al.[32] carried out experimental and numerical research to investigate the effect of N_2 and CO_2 dilution on premixed MTHF/ air flames characteristics. They found CO_2 has a more significant influence on flame speed reduction than N_2. To consider the effect of the high-temperature and the high-pressure environment in EGR technology. Kobayashi et al.[26] investigated the characteristics of CH_4/air turbulent premixed flame diluted with CO_2 at high pressure and high temperature, which corresponds to the EGR condition of a typical premixed gas turbine. Their research improved that the turbulent burning velocity was reduced with the CO_2 addition and indicated that the increase in the average volume of the flame zone and the decrease in the average fuel consumption rate produced by EGR effectively suppress the combustion oscillation premixed gas turbine combustor. Paidi et al.[27] analyzed the laminar burning velocity of H_2/air flame diluted with N_2/CO_2 at high temperatures. The results showed the effect of CO_2 dilution is greater than that of N_2 dilution in reducing the mixture's burning

velocity at higher temperatures. Their computational prediction is relatively consistent with the current experimental data. Lee et al.[28] investigated the effect of CO_2 dilution on flame stabilization, soot emissions, and combustion efficiencies of CH_4 jet flame at high pressure. The flame stabilization mechanism can be divided into the attached-flame regime, a lifted-flame regime, and the blow-off regime, most affected by the injected Reynolds number and fuel pipe depth. When the tip of the fuel pipe is moved into the intermediate oxidizer pipe, soot emissions under atmospheric pressure can be reduced, improving combustion efficiency. However, severe soot emissions occurred again under excessively high fuel flow rates and elevated pressures. In terms of instability control, CO_2 can effectively inhibit cellular instability[29] and combustion instability.[30,31]

In addition to CO_2 dilution, researchers have also researched other gas dilutions. Liu et al.[33] compared the effects of flame temperature controlled by Ar, N_2, and CO_2 dilution on the polycyclic aromatic hydrocarbons (PAHs) and soot formation in partially premixed and diffusion flames. They found that flame temperature significantly affected the evolution of PAHs and soot. The high-temperature area ranked in the order of $Ar > N_2 > CO_2$ at a high dilution flow rate, while the temperature distributions were similar at a low Ar, N_2, and CO_2 flow rate. Yi et al.[34] studied the effects of fuel properties on spray flames at oxygen-enriched conditions with multiple optical diagnostics. The results showed that the spray flame's shape, temperature, and species distributions strongly depended on oxygen concentration. Chu et al.[35] investigated the effects of N_2 dilution on laminar burning velocity (LBV), adiabatic flame temperature (AFT), intermediate radicals, and NOx emissions of rich methane/air premixed flames. Their results indicated the LBV, intermediate radicals, and NOx emissions first increased and then decreased as the equivalence ratio increased. The mole fraction of intermediate radicals and NOx decreased with the increase of the N_2 doping ratio under the same equivalence ratio. Yilmaz et al.[36] studied the effect of N_2 dilution on the instability and emission of a biogas flame. They found the dilution range of 20%–30% N_2 was the critical value of a biogas mixture containing 60% CH_4–40% CO_2. Stability remained unchanged after this critical value, and NOx and CO emissions increased significantly. Khanehzar et al.[37] simulated the effects of nitrogen and hydrogen addition/dilution on soot formation of laminar coflow ethylene/air diffusion flames with an in-house algorithm. The results indicated that mixing hydrogen and nitrogen into the fuel will reduce soot volume fraction and radiation. Soloklou et al.[38] conducted a simulation of the effect of H_2O dilution on NOx and CO formation in turbulent premixed CH_4/air flame with the k-ε/EDM framework. They illustrated that the energy absorbed by H_2O could cause a sharp drop in temperature and subsequent reductions in NOx and CO emissions.

Because at the upstream position, there are boundary conditions,[39] inlet thermodynamic properties,[40] flow fluctuations,[41] unstable fuel/air mixing, and equivalence ratio oscillation.[42–44] Thermoacoustic will become more frequent, and pollutant emissions will be out of balance.[45–47] So it is urgent to carry out corresponding research near the upstream position to control the thermoacoustic instability and the emission of pollutants.

Although there is a lot of research on the injection method to suppress combustion instability and NOx emissions,[11–15,30,31] to date, there is no research on the suppression of thermoacoustic instability and NOx emissions of unsteady swirl premixed flame with upstream microjets. In addition, most jet control methods are mainly based on modifying the combustion chamber structure, which may significantly limit the combustor's operating performance and combustion efficiency. In summary, combining the advantages of CO_2 and cross-flow jet in controlling combustion instability and pollutant emissions is necessary. Under the premise of not affecting the structure of the combustion chamber, carry out the corresponding CO_2 upstream microjets experiment.

This paper uses the upstream microjets method for the first time to control thermoacoustic instability and pollutant NOx emissions; the effects of CO_2 microjets flow rate, upstream microjets distance and microjets number on combustion instability and pollutant emissions were investigated through experiments. The dynamic pressure in the chamber, flame heat release rate and NOx emissions were analyzed synchronously in this study. Meanwhile, the flame mode was captured and subjected to post-processing analysis. This paper is organized as: The experimental procedures are depicted in Section 2. The results and discussion of measured parameters are presented in Section 3. Finally, the key findings are summarized in Section 4.

2 | EXPERIMENTAL PROCEDURES

2.1 | Geometric of the upstream microjets combustor

Figure 1 shows the schematic of the upstream microjets combustor used in this research. CH_4 and oxidant were uniformly mixed in the premixing plenum through the honeycomb during the experiment. The mixed flow is under the action of an axial cyclone with a swirl number

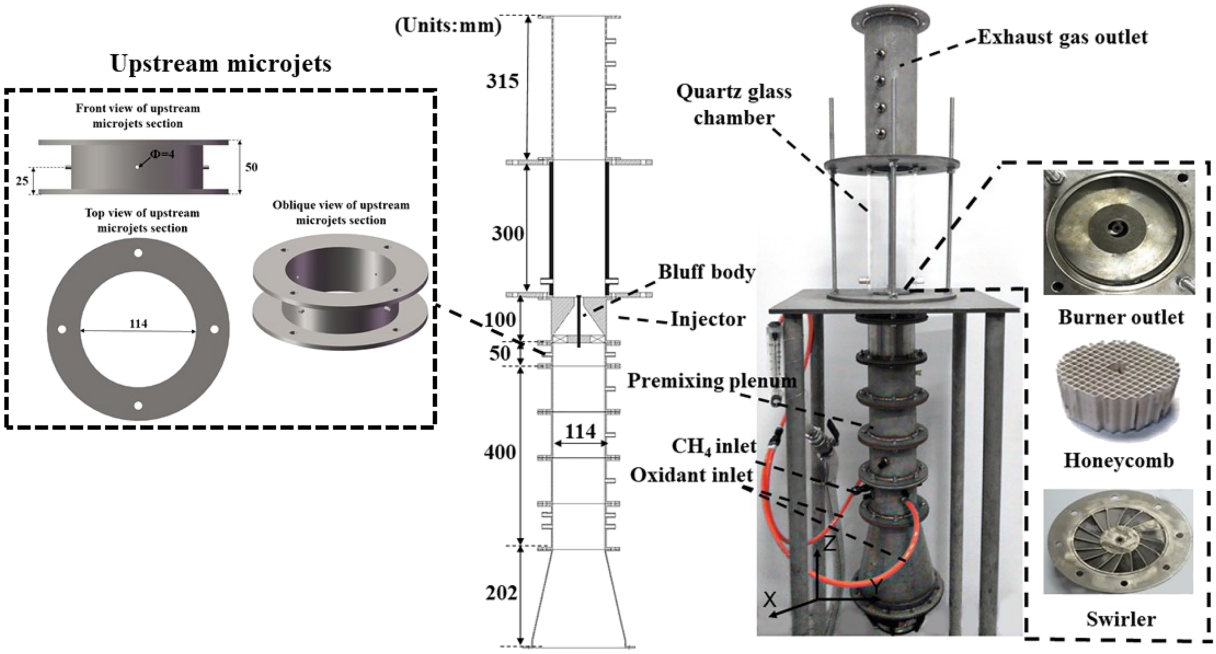

FIGURE 1 A schematic of the upstream microjets combustor

of 1.15,[31] and a strong swirl premixed flow is formed at the outlet of the burner injector. The high temperature resistant and transparent quartz glass chamber is used to observe flame changes. The ignition hole opened on the left side of the glass wall is used to ignite the premixed flow. A bluff body is placed in the center of the injector to stabilize the premixed flame. The threads tightly connect the various parts. The detailed geometric parameters of the upstream microjets combustor are present in Table 1.

The upstream microjets part as the core control part is placed at the upstream position 125 mm/225 mm/325 mm from the burner outlet plane. Four jet holes with 4 mm diameters are evenly distributed in the middle along the circumferential direction. The jet hole is smoothly opened on the inner cylindrical surface to eliminate the influence of the jet structure itself on the upstream flow field. Pneumatic connectors made of PVC are used to connect the CO_2 gas path and the upstream microjets part. At the same time, the cylindrical outer wall of the quartz glass chamber and exhaust gas outlet is provided with collection holes to collect the combustion chamber pressure and exhaust gas composition, respectively.

In Figure 2, the three-dimensional views of the unsteady model combustor under different orientations are drawn with the help of 3D modeling software. It can be seen from the partially enlarged view that the self-excited thermoacoustic oscillation of the burner can be realized under the close cooperation of the three core components of cyclone, bluff body and injector. In addition, according to the geometric dimensions of the burner in Table 1, the cut-off frequency f_c of the unsteady model combustor is about 1258 Hz.[31] Therefore, the sound waves in the pipe section propagate in one dimension.

TABLE 1 Geometric parameters of the upstream microjets combustor

Parameter	Value
Premixing plenum length (mm)	752
Combustion chamber length (mm)	300
Exhaust section length (mm)	315
Swirl number of the combustor	1.15
Diameter of the bluff body (mm)	11
The thickness of honeycomb (mm)	50
Diameter of upstream microjets (mm)	4

2.2 | Experimental setup

Figure 3 shows the systematic layout of measuring instruments for the upstream microjets experiments. The high-purity research-grade CH_4 (Purity: 99.995%) was used as fuel. The air compressor provided the oxidant part. The alicat mass flowmeter and air flowmeter were used to achieve flow control. The pressure sensor (CYG1406F, Bandwidth: 0–10 kPa) placed in the pressure measuring

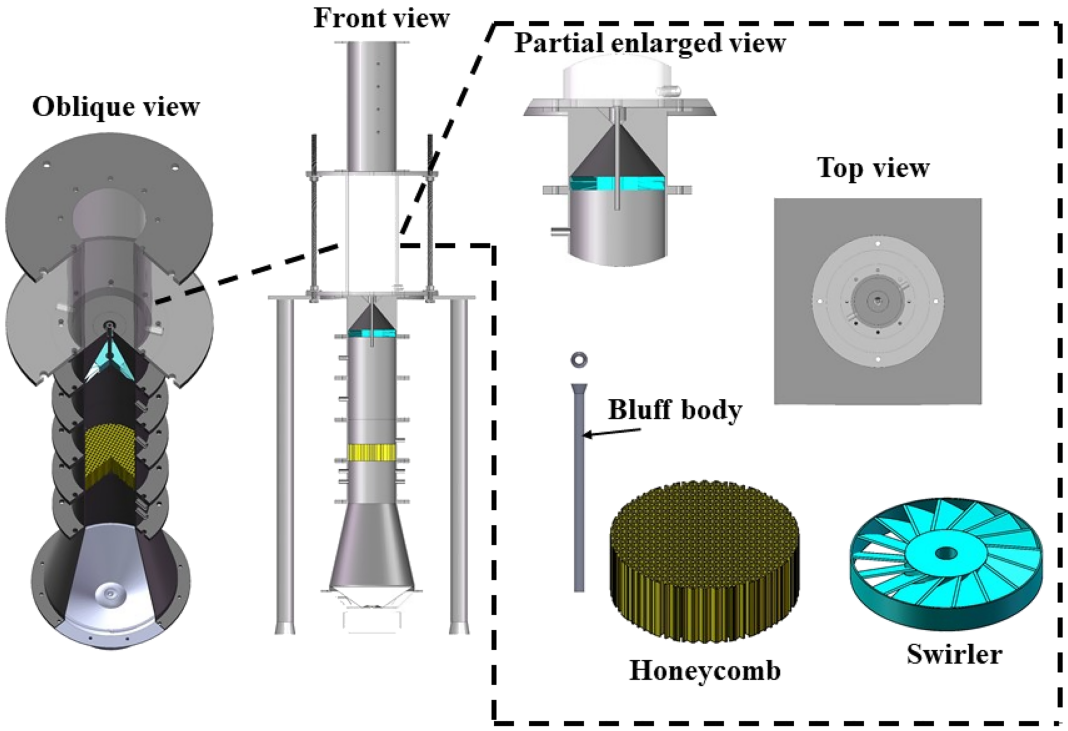

FIGURE 2 Three-dimensional views of the unsteady model combustor under different orientations

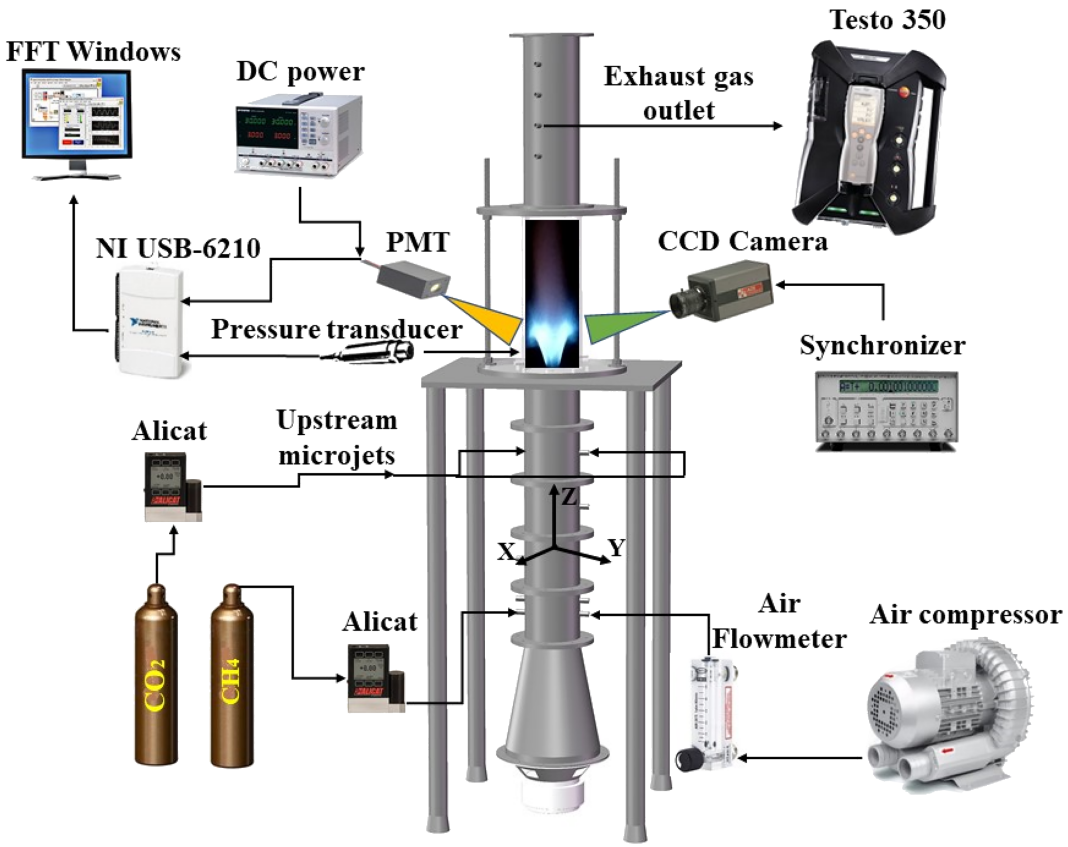

FIGURE 3 A systematic layout of measuring instruments for the upstream microjets experiments

hole at the height of 25 mm from the burner outlet plane is used to monitor the dynamic pressure changes in the combustion chamber. The synchronous change of flame heat release rate characterized by free radical CH* (430 ± 10 nm) was recorded by PMT (Hamamatsu H10722, photomultiplier tube). A transformer powers the pressure sensor. A DC power supply powers the PMT. The NI USB-6210 signal acquisition card is used to record the pressure and CH* dynamic changes before and after the upstream microjets control. The pressure and CH* signals saved in the Labview window of the computer desktop are used for analysis by the Origin FFT tool. The flame image was captured by a CCD camera (800 × 600 pixels resolution, pixel size: 14 μm) connected to a signal synchronizer (DG535 type). The flame length was analyzed with the Canny edge detection algorithm.[31] The TESTO 350 gas analyzer records the exhaust gas for NOx variation. The temperature field variations during the upstream microjets experiments were collected with a thermocouple (TM-902C K-type, 50°C–1300°C) at the axial center of 20 mm from the flame root.

The thermal power P and global equivalence ratio Φ_g were kept at 3.8 kW and 0.71, respectively, during the upstream microjets experiments. The CO_2 (Purity: 99.5%) is used as the jet medium. This paper analyzed the control feasibility of thermoacoustic instability and NOx emissions from three variables of upstream microjets flow rate, upstream microjets distance, and upstream microjets numbers. The specific operating conditions and the accuracy of the test equipment are present in Table 2 and Table 3.

3 | RESULTS AND DISCUSSION

Twelve upstream microjets configurations composed of different upstream microjets numbers 1/2/3/4 and upstream microjets distance 125/225/325 (mm) were designed during the experiments. For example, 1–125 means that the upstream microjets number is 1, and the upstream microjets distance is 125 mm. The flow rate of the CO_2 upstream microjets was changed from 0.0 to 1.0 L/min by an increment of 0.1 L/min. This paper clarifies the unsteady swirl premixed flame's dynamics and pollutant emission characteristics under different upstream microjets. Meanwhile, the temperature variation and the flame mode transition before and after upstream microjets control were also analyzed.

TABLE 2 Experimental conditions

Parameter	Value
Fuel type	Methane (99.995%)
Thermal power P (kW)	3.8
Global equivalence ratio (Φ_g)	0.71
Upstream microjets flow rate (L/min)	0.0–1.0
Upstream microjets distance (mm)	125/225/325
Number of upstream microjets	1/2/3/4
Upstream microjet pressure (Mpa)	0.105
Upstream microjet temperature (°C)	25
Upstream microjet medium	CO_2 (99.5%)

TABLE 3 Accuracy of the test equipment

Equipment	Accuracy
Dynamic Pressure Transducer	0.25%
Photomultiplier Tube	0.1%
TESTO 350 Gas Analyzer	±2%
Alicat Mass Flowmeter	0.2% FS
Air Flowmeter	1% FS
Thermocouple	± 2.5 °C

3.1 | Effect of upstream microjets distance

Figure 4 shows the variation of pressure amplitude in the chamber with microjets flow rate under different microjets numbers and distances: (a) one microjet, (b) two microjets, (c) three microjets, and (d) four microjets. The dynamic pressure amplitude in the chamber variation trend with jet flow rate under the same number of upstream microjets and different upstream microjets distances are compared and analyzed in each figure. With a minute amount of 0.1 L/min CO_2 injections, the dynamic pressure amplitude in the combustion chamber shows a rapid downward trend. The initial pressure damping speed $\overline{P}_i$ ((Pressure amplitude before control-pressure amplitude at 0.1 L/min)/0.1 L/min) is defined to compare the control effect under different jet configurations.

In most cases, the $\overline{P}_i$ decreases as the upstream microjet distance increases. In Figure 4a, the $\overline{P}_i$ of 1–125 reaches the maximum value of 259 Pa/(L/min); the pressure amplitude is suppressed from 52.4 Pa before control to 26.5 Pa. As the jet flow rate continues to increase, the pressure amplitude of the combustion chamber shows a downward trend as a whole, which proves the feasibility of the upstream microjets control method. There are fluctuations during the control period, which may be related to the fluctuation of the local equivalence ratio under the upstream microjets.[43]

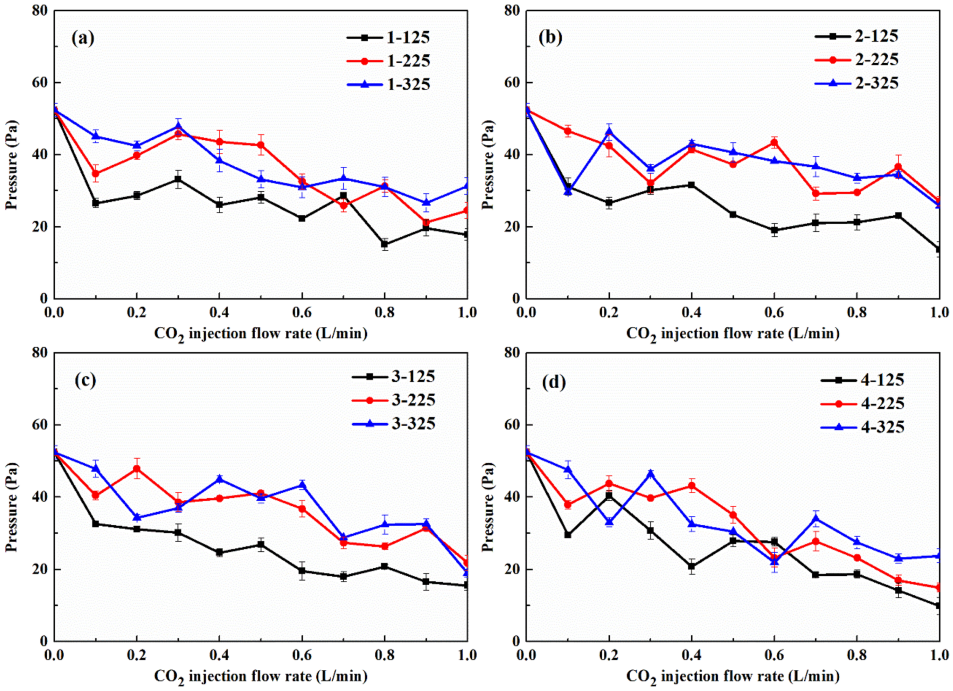

FIGURE 4 Variation of pressure amplitude in the chamber with microjets flow rate under different microjets numbers and distances. (a) One microjet, (b) two microjets, (c) three microjets, and (d) four microjets

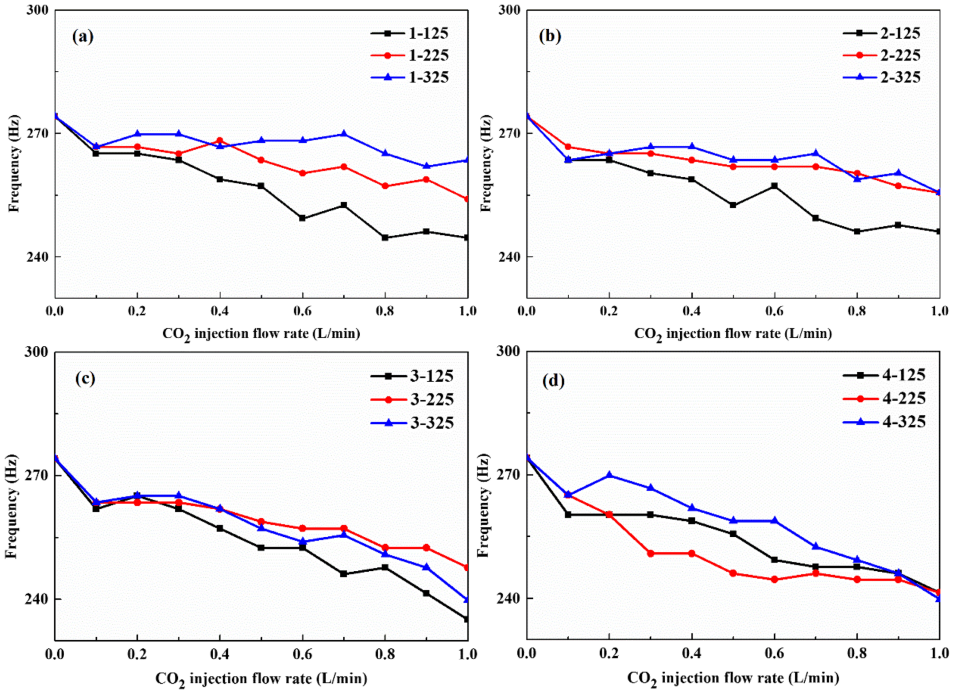

FIGURE 5 Shifting of pressure frequency in the chamber with microjets flow rate under different microjets numbers and upstream microjets distances. (a) One microjet, (b) two microjets, (c) three microjets, and (d) four microjets

The control effect is quantified by the suppression ratio d ((value before control-value after control)/value before control). In Figure 4d, the pressure suppression ratio d_p in the combustion chamber reaches the maximum value of 81.3% in 4–125 case, and the pressure value drops from 52.4 Pa to 9.8 Pa. The upstream microjets distance is inversely related to the pressure control effect, which may be associated with the flame-vortex interaction mechanism near the flame anchoring zone.[44] When the upstream distance is small, the rich vortex structure of the crossflow jet outlet[10] can more effectively promote the mixing of fuel and air about to enter the combustion chamber and suppress the flow rate fluctuations and equivalence ratio oscillations at the upstream position.[41–44]

Figure 5 shows the shifting of pressure frequency in the chamber with microjets flow rate under different microjets numbers and upstream microjets distances:

(a) one microjet, (b) two microjets, (c) three microjets, and (d) four microjets. The dominant frequency of the pressure in the chamber decreases as the microjets flow rate increases. The mode shift of frequency means that the coupling between flame and vortex is disturbed, and the phase difference between pressure and heat release is enlarged.[13] The thermoacoustic instability is suppressed, which is consistent with the conclusion in Figure 4. In Figure 5c, the pressure frequency suppression ratio in the combustion chamber reaches the maximum value of 11.9% in 3–125 case, which drops from 274.1 Hz to 241.4 Hz. Due to the high heat release rate and dilution of CO_2, the frequency of unstable combustion will decrease.[30]

Figure 6 shows the variation of CH* chemiluminescence intensity with microjets flow rate under different microjets numbers and upstream microjets distances: (a) one microjet, (b) two microjets, (c) three microjets, and (d) four microjets. With the increase of microjets flow rate, the CH* intensity in the combustion chamber overall shows a downward trend under different microjets numbers and upstream microjets distances. Define the initial CH* damping speed $\overline{H}_i$: (CH* intensity before control − CH* intensity at 0.1 L/min)/0.1 L/min. In Figure 6b, the $\overline{H}_i$ for 2–325 case reaches the maximum value of 0.046 arb.units/(L/min), and the CH* intensity drops from 0.007 arb.units before control to 0.0026 arb.units/(L/min). The reason may be the longer residence time when CO_2 is injected in the premixed plenum at a larger upstream distance. More CO_2 means more radiant heat release loss.[30] The suppression effect of CH* intensity in the combustion chamber is the largest when the upstream microjets distance is the smallest, and the control effect is not much different at other upstream microjets distances. The reason may be that the influence of CO_2 upstream microjets on heat release involves complex processes such as thermodynamics, fluid mechanics, and reaction kinetics.[3] The specific mechanism can be illustrated with the help of advanced tools such as PLIF, ICCD, and PIV in the future. In Figure 6c, the combustion chamber's CH* intensity suppression ratio d_{CH*} reached the maximum value of 80.2% in the 3–125 case, which dropped from 0.007 arb.units before control to 0.001 arb.units.

Figure 7 shows CH* chemiluminescence frequency shifting with microjets flow rate under different microjets numbers and upstream microjets distances: (a) one microjet, (b) two microjets, (c) three microjets, and (d) four microjets. The acoustic-heat release interaction mechanism is limited under CO_2 upstream microjets.[31] The heat release frequency shifts to a lower frequency as the CO_2 microjets flow rate increases. In Figure 7c, the CH* frequency suppression ratio reached the maximum value of 14.4% in 3–125 case, which drops from 274.5 Hz before control to 235.1 Hz.

The pressure and heat release show an attenuation trend under CO_2 upstream microjets, indicating the control feasibility of upstream microjets on thermoacoustic instability. In addition, different upstream microjets distances show other suppression effects, indicating that the upstream microjets distance is significant for the control effect.

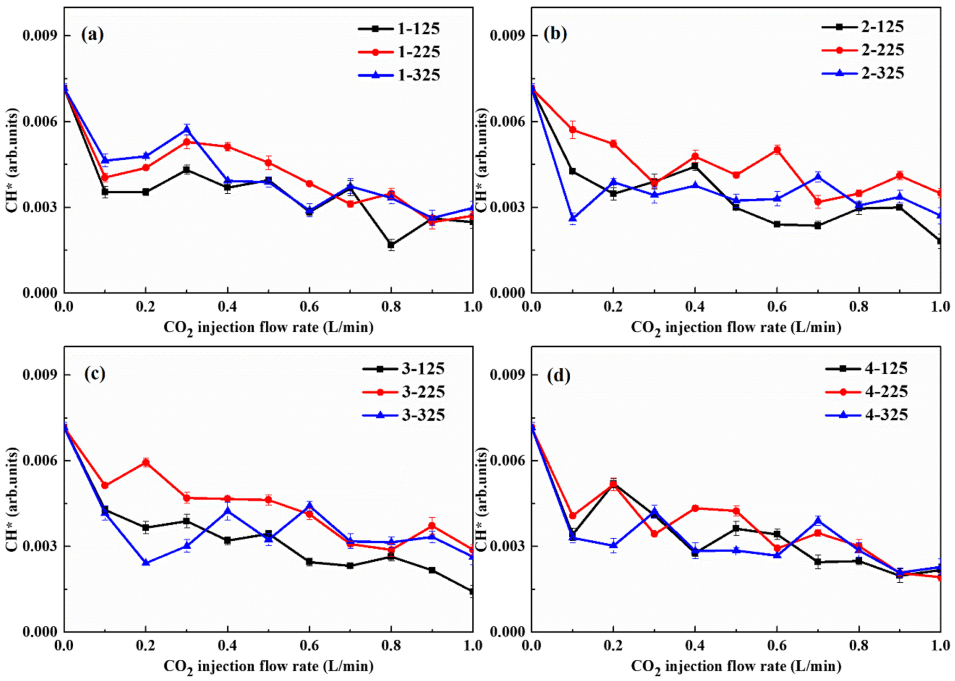

FIGURE 6 Variation of CH* chemiluminescence intensity with microjets flow rate under different microjets numbers and upstream microjets distances. (a) One microjet, (b) two microjets, (c) three microjets, and (d) four microjets

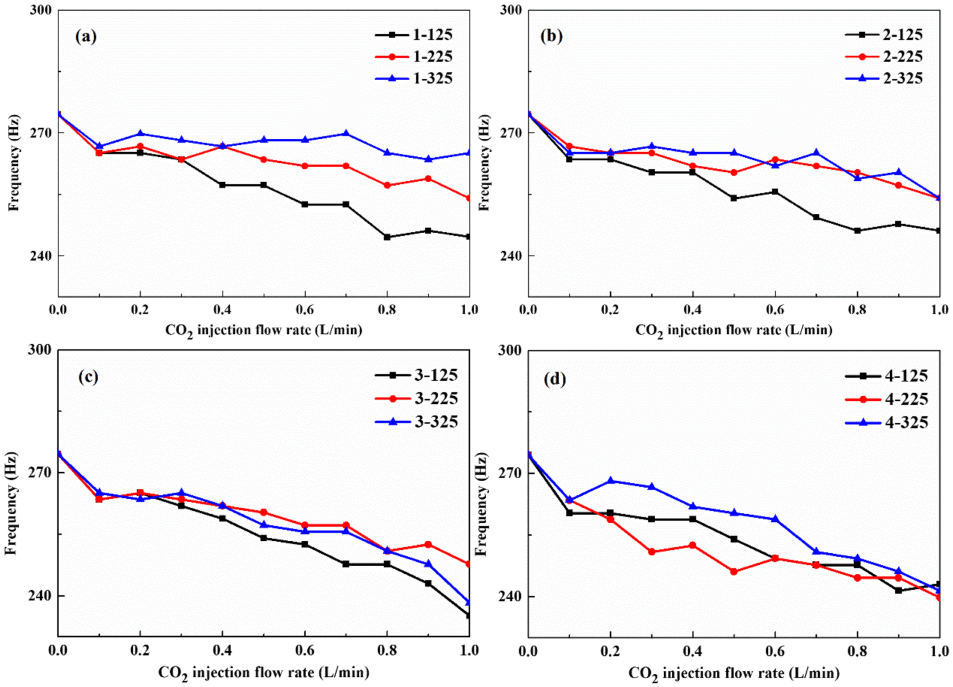

FIGURE 7 Shifting of CH* chemiluminescence frequency with microjets flow rate under different microjets numbers and upstream microjets distances. (a) One microjet, (b) two microjets, (c) three microjets, and (d) four microjets

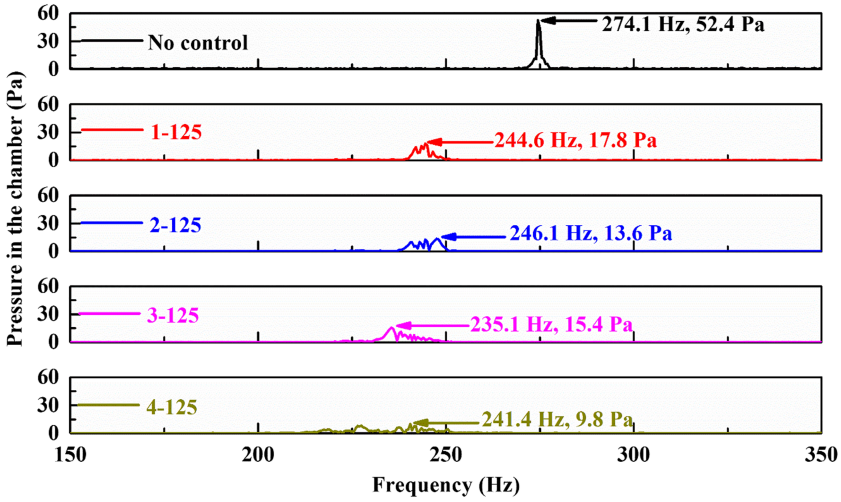

FIGURE 8 Pressure spectrum in the chamber under different microjets numbers when the microjets flow rate is 1.0 L/min, and the upstream microjets distance is 125 mm

3.2 | Effect of microjets numbers

Figure 8 and Figure 9 show the pressure and CH* spectrum under different microjets numbers when the microjets flow rate is 1.0 L/min, and the upstream microjets distance is 125 mm. In Figure 8, the pressure amplitude in the chamber is suppressed from 52.4 Pa to 9.8 Pa in 4–125 case. Meanwhile, the dominant pressure frequency in the chamber shifts from 274.1 Hz to 241.4 Hz. In Figure 9, the CH* intensity is suppressed from 0.007 arb. units to 0.001 arb.units in 3–125 case, and the dominant CH* frequency shifts from 274.5 Hz to 235.1 Hz. The dynamic pressure and heat release under different microjets numbers cases are suppressed, but the control effect is not much different.

3.3 | NOx emissions characteristics

Figure 10 shows the variation of NOx emissions with microjets flow rate under different microjets numbers and distances: (a) one microjet, (b) two microjets, (c) three microjets, and (d) four microjets. The NOx emissions in the exhaust gas decrease as the microjets flow rate increases. The NOx emissions show a downward trend as the flow rate increases. The change of NOx undergoes a stable period due to the limited content of CO_2 concentration at a flow rate of 0.1–0.5 L/min. The NOx drops rapidly as the flow continues to increase. The NOx suppression effect is proportional to the upstream distance; the larger the distance, the greater the NOx suppression effect. The reason may be due to the longer time

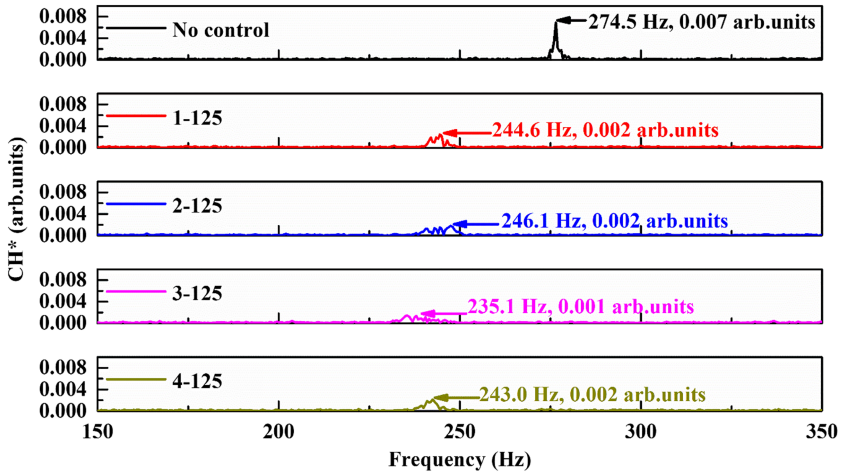

FIGURE 9 CH* chemiluminescence spectrum under different microjets numbers when the microjets flow rate is 1.0 L/min, and the upstream microjets distance is 125 mm

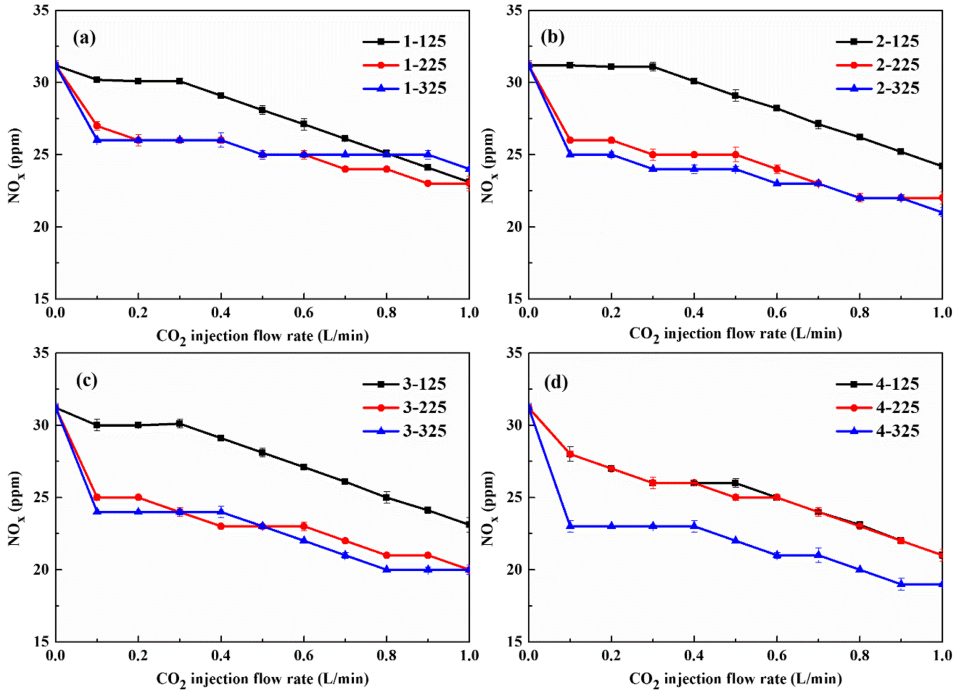

FIGURE 10 Variation of NOx emissions with microjets flow rate under different microjets numbers and distances. (a) One microjet, (b) two microjets, (c) three microjets, and (d) four microjets

that CO_2 stays in the premixed plenum in the case of a larger upstream distance. Due to its excellent physical and chemical properties,[19–22] CO_2 with a high radiation heat transfer coefficient can effectively reduce the flame temperature and NOx emissions. In Figure 10d, the NOx emissions decrease from 31.2 ppm to 19.0 ppm in 4–325 case, reaching the maximum reduction of 12.2 ppm. It shows that NOx emissions can be effectively reduced with a minute CO_2 injected from the upstream. At the same time, it can be seen from the results in Section 3.2 that thermoacoustic instability is also gradually attenuated under the action of CO_2 upstream microjets. Therefore, CO_2 upstream microjets can effectively realize the coordinated control of thermoacoustic instability and NOx emissions.

To analyze the real-time changes of the temperature field in the combustion chamber under CO_2 upstream microjets. A K-type thermocouple was fixed in the combustion chamber at a center distance of 20 mm from the flame root. Figure 11 shows the temperature variation with the microjets flow rate at the center of 30 mm from the flame root under different upstream microjets distances when the microjets numbers are 4. The temperature drops from 1296.2 K to 1257.4 K in 4–325 case, achieving the maximum reduction of 38.8 K. The suppression effect of the combustion chamber temperature is proportional to the upstream distance. The larger the upstream distance, the more pronounced decrease of the temperature. At the same time, when the CO_2 concentration is between 0.6 and 0.1 L/min, the

temperature drop speed increases, which shows that the temperature drop is related to the upstream distance and the CO_2 concentration. These results correspond to the changing trend of NOx under the action of CO_2 upstream microjets; it shows the importance of temperature changes to NOx emissions. With the increase of CO_2 flow rate, the temperature in the combustion chamber shows a downward trend, reducing the thermal NOx emissions.[24,25,31] Meanwhile, the combustion reaction is also dampened and then restrained the heat release.[30] Finally, the phase between acoustic and heat release oscillations is out of phase, suppressing the thermoacoustic instability coupling mechanism.[1–3]

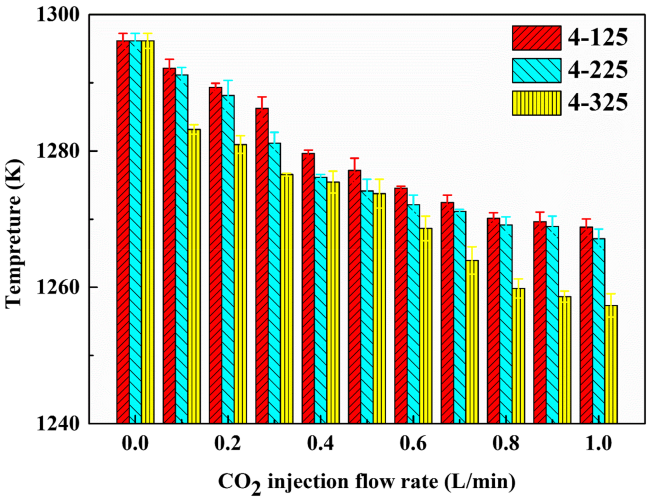

FIGURE 11 Variation of temperature with the microjets flow rate at the center of 30 mm from the flame root under different upstream microjets distances when the microjets numbers are 4

3.4 | Evolution of flame mode

Figure 12 shows the variation of flame macrostructure with the microjets flow rate under different upstream microjets distances when the microjets numbers are 4. The flame luminosity gradually darkens with the increase of CO_2 injection flow rate, which may be the reason for the decrease of certain free radicals in the flame.[22,30] At the same time, the flame shape has also changed accordingly. The inner and outer recirculation zones are transformed, which may result in a different turbulent stretch rate and burning velocity.[14,31] The fluid-acoustic-flame interaction mechanism is disturbed under the upstream microjets, and the vortex shedding frequency will shift, inducing a new acoustic frequency.[2,3] Moreover, the flame front obviously shrinks in 4–225 and 4–325 cases. The residence time of flame will be reduced, suppressing the formation of NOx.[30,31] The flame becomes more compact, and the combustion is more stable, which helps to build a safe and small burner.

To better characterize the change of flame shape under CO_2 upstream microjets, use the Canny edge detection algorithm of MATLAB software to calculate the flame length. Figure 13 shows the variation of flame macrostructure with the microjets flow rate under different upstream microjets distances when the microjets numbers are 4. The flame length decreased significantly under the CO_2 upstream microjets of 0.0–0.4 L/min. As the CO_2 flow rate continues to increase, the flame length slowly decreases. Among them, the flame length is reduced from 112 mm before control to 106 mm in 4–125 case, achieving a 6 mm reduction. The flame length is reduced from 112 mm before control to 101 mm in 4–225 case, achieving an 11-mm reduction. The flame length is reduced from 112 mm before control to 98 mm in 4–325 case, achieving a 14-mm reduction. It can be seen that the

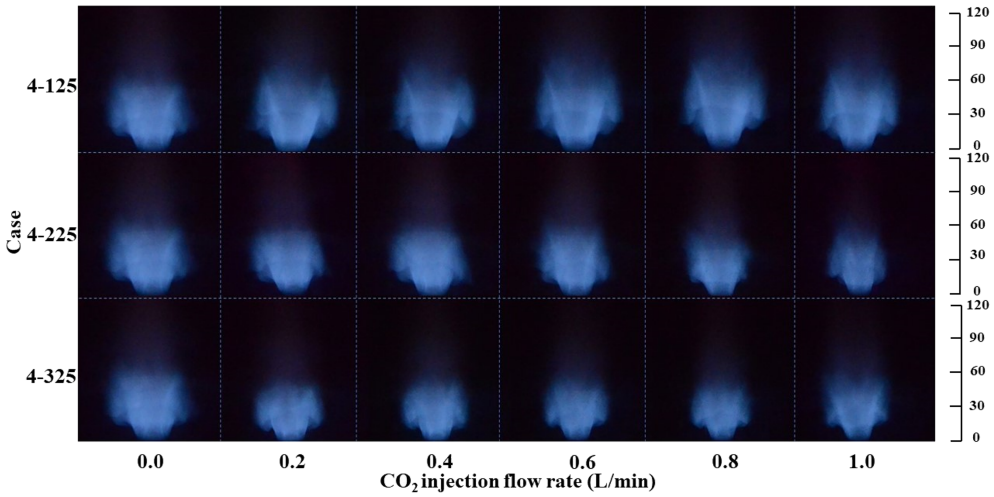

FIGURE 12 Variation of flame macrostructure with the microjets flow rate under different upstream microjets distances when the microjets numbers are 4

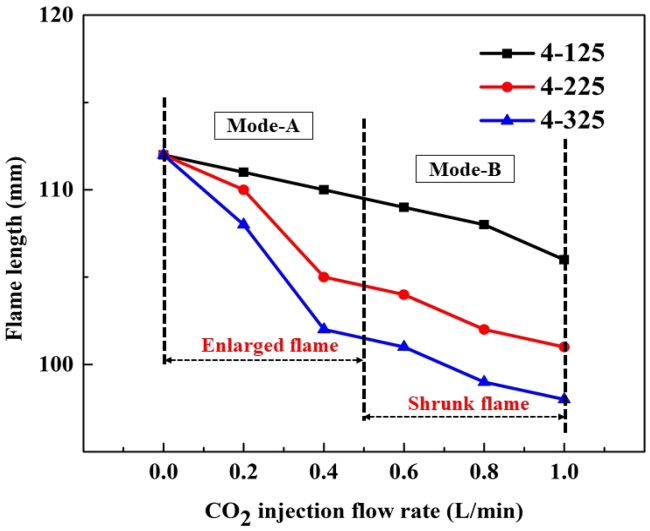

FIGURE 13 Variation of flame length with the microjets flow rate under different upstream microjets distances when the microjets numbers are 4

greater the upstream microjets distances, the more significant decrease in flame length, which may be related to the CO_2 residence time.[24] A larger upstream microjets distance means CO_2 stays longer in the premixed plenum, and the flame temperature will be significantly reduced.[19–22,30] At the same time, due to the influence of lateral microjets, the flame turbulence velocity will likely become larger, making the flame length shorter.[31] Two flame forms were defined: Mode-A and Mode-B, which combine the thermoacoustic characteristics and the change of flame macrostructure. In Mode-A, the flame is in a state of unstable combustion and presents an enlarged flame shape. In Mode-B, the flame is in a stable combustion state. The inner and outer recirculation zone and the flame front are contracted, and the pollutant NOx is also significantly reduced, showing a shrunk flame shape. The characterization of the above two flame modes helps define the combustion and pollutant emission characteristics under CO_2 upstream microjets.

4 | CONCLUSIONS

This paper investigated the effect of upstream microjets on suppressing thermoacoustic instability and NOx emissions of unsteady swirl premixed flame. Three variables of upstream microjets were analyzed-microjets flow rate, upstream microjets distance, and microjets number. The results proved the synergistic control feasibility of upstream microjets on thermoacoustic instability and pollutant NOx emissions. Meanwhile, some discoveries of upstream microjets in unsteady combustion and pollutant emissions will promote its practical application in gas turbine systems. In the best upstream microjets case, the pressure suppression ratio in the combustion chamber can reach the maximum value of 81.3%. The CH* suppression ratio reaches the maximum value of 80.2%. In addition to changes in pressure and heat release amplitude, the frequency of pressure and heat release has also changed from high frequency to low frequency, avoiding the phenomenon of high-frequency and high-amplitude thermoacoustic instability. The NOx emissions can reach the maximum reduction of 12.2 ppm. With the increase of CO_2 upstream microjets flow rate, the flame presents two flame modes: Mode-A: enlarged flame and Mode-B: shrunk flame. The flame length becomes shorter; the maximum reduction can reach 14 mm. Meanwhile, it is found that the thermoacoustic phenomenon is more wholly suppressed when the upstream distance is smaller. When the upstream distance is larger, the pollutant NOx is reduced more completely, which means that an optimized and compromised strategy needs to be adopted to coordinate the control of thermoacoustic instability and pollutant NOx emissions. Thermoacoustic instability often involves kinetics, hydrodynamics, thermodynamics, molecular transport, and acoustics. As for the detailed changes of the turbulent field, space heat release rate, and chemical-free radicals under the control of CO_2 upstream microjets, advanced visualization tools such as PIV, ICCD, and PLIF will be used for in-depth exploration in the future. The CO_2 upstream microjets method used in this paper only involves the structural modification in the upstream premixed plenum without modifying the complex combustion chamber structure, which will help realize a simple-efficient and economical-practical control strategy.

ACKNOWLEDGEMENT

This work was supported by the National Science Fund for Distinguished Young Scholars (grant number 51825605).

NOMENCLATURE

S	swirl number of upstream microjets combustor
f_c	cut-off frequency of upstream microjets combustor, Hz
P	thermal power, kW
Φ_g	global equivalent ratio
$\overline{P}_i$	the initial pressure damping speed, Pa/(L/min)
d	the suppression ratio, %
d_p	the pressure suppression ratio, %
d_{pf}	the pressure frequency suppression ratio, %

$\overline{H_i}$ the initial CH* damping speed, arb.units/(L/min)
d_{CH*} the CH* suppression ratio, %
d_{CH*f} the CH* frequency suppression ratio, %

ORCID

Hao Zhou https://orcid.org/0000-0001-9779-7703

REFERENCES

1. Rayleigh L. The explanation of certain acoustical phenomena. *Nature*. 1878;18(455):319-321.
2. Poinsot T. Prediction and control of combustion instabilities in real engines. *Proc Combust Inst*. 2016;36:1-28.
3. Huang Y, Yang V. Dynamics and stability of lean-premixed swirl-stabilized combustion. *Prog Energy Combust Sci*. 2009;35(4):293-364.
4. Hughes IJ, Dowling AP. The absorption of sound by perforated linings. *J Fluid Mech*. 2006;218(218):299-335.
5. Oh S, Shin Y, Kim Y. Stabilization effects of perforated plates on the combustion instability in a lean premixed combustor. *Appl Therm Eng*. 2016;107:508-515.
6. Park IS, Sohn CH. Nonlinear acoustic damping induced by a half-wave resonator in an acoustic chamber. *Aerosp Sci Technol*. 2010;14(6):442-450.
7. Sohn CH, Park JH. A comparative study on acoustic damping induced by half-wave, quarter-wave, and Helmholtz resonators. *Aerosp Sci Technol*. 2011;15(8):606-614.
8. Harrje DT & Reardon FH Liquid propellant rocket combustion instability. NASA SP-194, NASA Special Publication 194, 1972.
9. Zhao D, Li XY. A review of acoustic dampers applied to combustion chambers in aerospace industry. *Prog Aerosp Sci*. 2015;74:114-130.
10. Mahesh K. The interaction of jets with crossflow. *Annu Rev Fluid Mech*. 2013;45(1):379-407.
11. Choi GM, Tanahashi M, Miyauchi T. Control of oscillating combustion and noise based on local flame structure. *Proc Combust Inst*. 2005;30(2):1807-1814.
12. Ghoniem AF, Annaswamy A, Park S, Sobhani ZC. Stability and emissions control using air injection and H_2 addition in premixed combustion. *Proc Combust Inst*. 2005;30(2):1765-1773.
13. Murat Altay H, Hudgins DE, Speth RL, Annaswamy AM, Ghoniem AF. Mitigation of thermoacoustic instability utilizing steady air injection near the flame anchoring zone. *Combust Flame*. 2010;157(4):686-700.
14. LaBry ZA, Shanbhogue SJ, Speth RL, Ghoniem AF. Flow structures in a lean-premixed swirl-stabilized combustor with microjet air injection. *Proc Combust Inst*. 2011;33(1):1575-1581.
15. Altay M, Speth R, Snarheim D, Hudgins D, Ghoniem A, Annaswamy A. Impact on microjet actuation on stability of a backward-facing step combustor. 45th AIAA Aerospace Sciences Meeting and Exhibit. 2007.
16. Verschaeren R, Schaepdryver W, Serruys T, Bastiaen M, Vervaeke L, Verhelst S. Experimental study of NOx reduction on a medium speed heavy duty diesel engine by the application of EGR (exhaust gas recirculation) and Miller timing. *Energy*. 2014;76:614-621.
17. Tornatore C, Bozza F, De Bellis V, Teodosio L, Valentino G, Marchitto L. Experimental and numerical study on the influence of cooled EGR on knock tendency, performance and emissions of a downsized spark-ignition engine. *Energy*. 2019;172:968-976.
18. Zheng Z, Yue L, Liu H, Zhu Y, Zhong X, Yao M. Effect of two-stage injection on combustion and emissions under high EGR rate on a diesel engine by fueling blends of diesel/gasoline, diesel/n-butanol, diesel/gasoline/n-butanol and pure diesel. *Energ Convers Manage*. 2015;90:1-11.
19. Gascoin N, Yang Q, Chetehouna K. Thermal effects of CO_2 on the NOx formation behavior in the CH_4 diffusion combustion system. *Appl Therm Eng*. 2017;110:144-149.
20. Wang D, Ji C, Wang S, Meng H, Yang J. Chemical effects of CO_2 dilution on CH_4 and H_2 spherical flame. *Energy*. 2019;185:316-326.
21. Yang J, Gong Y, Guo Q, Zhu H, He L, Yu G. Dilution effects of N_2 and CO_2 on flame structure and reaction characteristics in CH_4/O_2 flames. *Exp Therm Fluid Sci*. 2019;108:16-24.
22. Zhao X, Shi B, Peng W, et al. Effects of N_2 and CO_2 dilution on the combustion characteristics of C_3H_8/O_2 mixture in a swirl tubular flame burner. *Exp Therm Fluid Sci*. 2019;100:251-258.
23. Hasti VR, Lucht RP, Gore JP. Large eddy simulation of hydrogen piloted CH_4/air premixed combustion with CO_2 dilution. *J Energy Inst*. 2020;93(3):1099-1109.
24. Soloklou MN, Golneshan AA. Effect of CO_2 diluent on the formation of pollutant NOx in the laminar non-premixed methane-air flame. *Int J Heat Mass Transf*. 2019;148:119071
25. Min CL, Seo SB, Yoon J, Kim M, Yoon Y. Experimental study on the effect of N_2, CO_2, and steam dilution on the combustion performance of H_2 and CO synthetic gas in an industrial gas turbine. *Fuel*. 2012;102:431-438.
26. Kobayashi H, Hagiwara H, Kaneko H, Ogami Y. Effects of CO_2 dilution on turbulent premixed flames at high pressure and high temperature. *Proc Combust Inst*. 2007;31(1):1451-1458.
27. Paidi SK, Bhavaraju A, Akram M, Kumar S. Effect of N_2/CO_2 dilution on laminar burning velocity of H_2–air mixtures at high temperatures. *Int J Hydrogen Energy*. 2013;38(31):13812-13821.
28. Lee J, Hwang GJ, Lee JI, Jamal A, Kim NI. Flame stabilization and soot emission of methane jet flames for CO_2 diluted oxy-combustion at elevated pressure. *Combust Flame*. 2021;231:111490
29. Wei S, Yu M, Pei B, Zhu Z, Zhang Z. Suppression of CO_2 and H_2O on the cellular instability of premixed methane/air flame. *Fuel*. 2020;264:116862
30. Lee K, Kim H, Park P, Yang S, Ko Y. CO_2 radiation heat loss effects on NOx emissions and combustion instabilities in lean premixed flames. *Fuel*. 2013;106:682-689.
31. Tao C, Zhou H. Dilution effects of CO_2, Ar, N_2 and He microjets on the combustion dynamic and emission characteristics of unsteady premixed flame. *Aerosp Sci Technol*. 2021;111:106537
32. Sahu A, Wang C, Jiang C, et al. Effect of CO_2 and N_2 dilution on laminar premixed MTHF/air flames: Experiments and kinetic studies. *Fuel*. 2019;255:115659
33. Liu H, Cui Y, Chen B, et al. Effects of flame temperature on PAHs and soot evolution in partially premixed and diffusion flames of a diesel surrogate. *Energy Fuel*. 2019;33(11):11821-11829.

34. Yi W, Liu H, Feng L, et al. Multiple optical diagnostics on effects of fuel properties on spray flames under oxygen-enriched conditions. *Fuel*. 2021;291:120129
35. Chu H, Xiang L, Meng S, Dong W, Gu M, Li Z. Effects of N_2 dilution on laminar burning velocity, combustion characteristics and NOx emissions of rich CH_4–air premixed flames. *Fuel*. 2021;284:119017
36. Yilmaz I, Cam Y, Alabas B. Effect of N_2 dilution on combustion instabilities and emissions in biogas flame. *Fuel*. 2022;308:121943
37. Khanehzar A, Cepeda F, Dworkin SB. The influence of nitrogen and hydrogen addition/dilution on soot formation in coflow ethylene/air diffusion flames. *Fuel*. 2022;309:122244
38. Soloklou MN, Golneshan AA. Numerical study of the effect of H_2O diluents on NOx and CO formation in turbulent premixed methane-air flame. *Int J Hydrogen Energy*. 2020;45(18):10882-10894.
39. Han X, Yang D, Wang J, Zhang C. The effect of inlet boundaries on combustion instability in a pressure-elevated combustor. *Aerosp Sci Technol*. 2021;111:106517
40. Li W, Zhao D, Chen X, et al. Numerical investigations on solid-fueled ramjet inlet thermodynamic properties effects on generating self-sustained combustion instability. *Aerosp Sci Technol*. 2021;119:107097
41. Pillai AL, Nagao J, Awane R, Kurose R. Influences of liquid fuel atomization and flow rate fluctuations on spray combustion instabilities in a backward-facing step combustor. *Combust Flame*. 2020;220:337-356.
42. Lieuwen TC, Yang V. *Combustion Instabilities in Gas Turbine Engines: Operational Experience, Fundamental Mechanisms, and Modeling*. USA: AIAA Inc.; 2005.
43. Murat Altay H, Speth RL, Hudgins DE, Ghoniem AF. The impact of equivalence ratio oscillations on combustion dynamics in a backward-facing step combustor. *Combust Flame*. 2009;156(11):2106-2116.
44. Zhao H, Li G, Zhao D, et al. Experimental study of equivalence ratio and fuel flow rate effects on nonlinear thermoacoustic instability in a swirl combustor. *Appl Energ*. 2017;208:123-131.
45. Yilmaz H, Yilmaz I. Combustion and emission characteristics of premixed $CNG/H_2/CO/CO_2$ blending synthetic gas flames in a combustor with variable geometric swirl number. *Energy*. 2019;172:117-133.
46. Souflas K, Perrakis K, Koutmos P. On the turbulent flow and pollutant emission characteristics of disk stabilized propane-air flames, under inlet mixture stratification and preheat. *Fuel*. 2020;260:116333
47. Han W, Li B, Pan S, Lu Y, Li X. Combined effect of inlet pressure, total cycle energy, and start of injection on low load reactivity controlled compression ignition combustion and emission characteristics in a multi-cylinder heavy-duty engine fueled with gasoline/diesel. *Energy*. 2018;165:846-858.

How to cite this article: Hu L, Zhou H. Suppression of thermoacoustic instability and NOx emissions of unsteady swirl premixed flame with upstream microjets. *Asia-Pac J Chem Eng*. 2022;17(2):e2744. doi:10.1002/apj.2744